Supporting Information

Anodic Electrochemical C–C Bond Cleavage Co-Catalyzed by Ionic Liquids and FeNi@C for Lignin Upgrading

Weiwei Wang, ‡[a, c], Yuqing Zhai, ‡ [b], Xiaoyan Ji [d], Hao Wang [a, b*], and Yanrong Liu [a, b, c*]

[a] CAS Key Laboratory of Green Process and Engineering, State Key Laboratory of Mesoscience and Engineering, Beijing Key Laboratory of Ionic Liquids Clean Process, Institute of Process Engineering, Chinese Academy of Sciences, Beijing 100190, China

[b] Longzihu New Energy Laboratory, Zhengzhou Institute of Emerging Industrial Technology, Henan University, Zhengzhou 450000, P. R. China

[c] School of Chemical Engineering, University of Chinese Academy of Sciences, Beijing 100049, China

[d] Energy Engineering, Division of Energy Science, Luleå University of Technology, Luleå 97187, Sweden

‡ These authors contributed to this work equally.

E-mail: yrliu@ipe.ac.cn; haowang@ipe.ac.cn.

Materials

$FeCl_3 \cdot 6H_2O$ (AR) was obtained from Tianjin Damao Chemical Reagent Factory. $NiCl_2 \cdot 6H_2O$ (99%), terephthalic acid (BDC, 99%), 1-butyl-3-methylimidazolium chloride (BmimCl, 98%), 1-butyl-1-methylpyrrolidinium chloride (BmpyrroCl, 98%), 1-butylpyridinium chloride (BmpyriCl, 99%), 1-butyl-3-methylimidazolium bromide (BmimBr], 99%), and N,N-dimethylformamide (DMF, 99.8%) were purchased from Adamas Reagent Co., Ltd.,, Shanghai. Pt/C (Pt 60 wt%) was purchased from Suzhou Senelone Technology Co., Ltd. Veratrylglycerol-β-guaiacyl ether (VG, 97%), veratraldehyde (VAld, 98%), veratric acid (VAc, 98%), and guaiacol (99%), 1-butyl-3-methylimidazolium trifluoromethanesulfonate (BmimOTF, 98%) were also obtained from Beijing Innochem Technology Co., Ltd.

Preparation of FeNi@C

In a clean beaker, 35 ml of DMF, 0.4 mM BDC, 0.2 mM $NiCl_2 \cdot 6H_2O$, and 0.2 mM $FeCl_3 \cdot 6H_2O$ were mixed and stirred for 30 minutes until dissolved. Subsequently, 2.5 ml of anhydrous ethanol and 2.5 ml of ultrapure water were pre-mixed and added to the solution, which was then stirred thoroughly. The mixture was transferred into a reaction vessel with a polytetrafluoroethylene lining and pre-treated nickel foam was added. The reaction was conducted at 125°C for 12 hours. After cooling to room temperature, the FeNi-BDC precursor grown in situ on the nickel foam was alternately washed three times with ethanol and deionized water and vacuum-dried at 70°C overnight. The FeNi-BDC was carbonized at 600°C for 2 hours under an argon atmosphere at a heating rate of 3°C/min to obtain NiFe@C. Ni@C was prepared using the same procedure by replacing $FeCl_3 \cdot 6H_2O$ with an equimolar amount of $NiCl_2 \cdot 6H_2O$. Similarly, Fe@C was prepared by substituting $NiCl_2 \cdot 6H_2O$ with an equimolar amount of $FeCl_3 \cdot 6H_2O$.

Characterization

X-ray diffraction (XRD) patterns were recorded on a Rigaku SmartLab SE instrument using Cu Kα radiation (λ = 1.5418 Å), with a scanning range of 10° to 90° and a step size of 5°. Microstructural analysis was performed using a Talos F200x transmission electron microscope (TEM) from FEI at an accelerating voltage of 200

kV. Scanning electron microscopy (SEM) equipped with energy-dispersive X-ray spectroscopy (EDS) on a GeminiSEM 300 was used to analyze the microstructure and elemental composition of the electrocatalysts. X-ray photoelectron spectroscopy (XPS) was conducted on a Thermo Scientific K-Alpha instrument using Al Kα radiation (1486.6 eV) to elucidate the surface chemical states, with the C1s binding energy set at 284.8 eV for calibration. Fourier-transform infrared (FT-IR) spectra were acquired using a Bruker INVENIO S spectrometer. Raman spectra were obtained using a HORIBA XploRA PLUS Raman spectrometer, covering a wavenumber range of 100-2000 cm^{-1}. The GCMS-QP2010 Ultra instrument was employed for qualitative analysis of the product, with a 1 μl sample injection and a split ratio of 20:1. The temperature program involved ramping from room temperature to 40°C, holding at 40°C for 1 minute, and then increasing to 300°C at a rate of 10 °C/min, followed by a final hold at 300°C for 5 minutes. High-resolution liquid chromatography-mass spectrometry (HR-LC-MS) of the products was performed using a Trip Tof 5600+ from AB Sciex. The quantification of VAld and VAc in the products was determined by high-performance liquid chromatography (HPLC) on an Alliance e2695 system. Electron spin resonance (ESR) experiments were conducted on an EMXplus-9.5/12 spectrometer to capture free radicals, using 5,5-dimethyl-1-pyrroline N-oxide (DMPO) as a spin trap to detect spin-active species •OH and $•O_2^-$ in the catalyst or aqueous solution.

Electrochemical characterization

The electrochemical performance of the prepared catalysts was evaluated using a PARSTAT 3000A-DX electrochemical workstation in a standard three-electrode configuration. A Pt plate served as the counter electrode, Hg/HgO as the reference electrode, and FeNi@C served as the working electrode. The Hg/HgO reference electrode was calibrated to the reversible hydrogen electrode (RHE, 0.860 V) potential in a hydrogen-saturated 0.5 M KOH + 0.05 mM VG electrolyte, with all potentials reported vs. RHE unless otherwise stated. Linear sweep voltammetry (LSV) was performed at a scan rate of 5 mV/s over a potential range of 1.2 to 1.7 V vs. RHE. Electrochemical impedance spectroscopy (EIS) measurements were carried out under

constant voltage conditions across a frequency range of 0.1 to 10^5 Hz. Chronoamperometry at a constant potential was used to evaluate the catalyst's VG conversion efficiency and VAld selectivity.

For anion exchange membrane (AEM) electrolyzer testing, 60 wt% Pt/C and FeNi@C were used as the cathode and anode electrocatalysts, respectively. The Pt/C catalyst was dispersed in a mixed solvent of water and isopropanol (3:2 v/v), and Nafion 117 solution was added to achieve an ionomer-to-catalyst weight ratio of 0.9:1. The mixture was ultrasonicated in an ice bath for 1 h and then sonicated sprayed onto a Tarray 060 carbon paper at a rate of 0.3 ml/min to form a cathode electrode with a 4 cm^2 effective area and a platinum loading of 0.2 mg (Pt)/cm^2. Self-supported FeNi@C was directly used as the anode electrode. The electrodes were assembled on both sides of a PiperION A40-HCO3 anion exchange membrane. All AEM electrolyzer performance tests were conducted using a Gamry Reference 3000 instrument equipped with a 30k booster. Polarization curves were obtained by LSV from 1.2 to 1.8 V at a scan rate of 10 mV/s. Chronoamperometry was performed at 1.4 V with 0.5 M KOH + 0.5 mM VG electrolyte on the anode side and 0.5 M KOH electrolyte on the cathode side. To investigate the synergistic catalysis with ionic liquids (ILs), an additional 0.26 g of BmpyrroCl was incorporated into the anode-side electrolyte, and the other experimental conditions remained unchanged.

BmpyrroCl was recycled to validate its stability after 5 consecutive chronoamperometric tests. Each test was conducted at 1.4 V for 3 h. The recycling procedure for BmpyrroCl involved the extraction of reaction products from the electrolyte using ethyl acetate, followed by centrifugation to separate the aqueous phase containing unreacted impurities. This process was repeated three times. Subsequently, water was removed via rotary evaporation to recover the ILs and KOH electrolyte. For the next cycle, water is added to formulate a fresh electrolyte, and a small amount of KOH is introduced to adjust the pH of the electrolyte to 13 and the solution is brought to a final volume of 25 ml.

Computational details

Density functional theory as implemented in the Vienna Ab-initio Simulation Package (VASP) was employed to optimize the geometric structures [1, 2]. The exchange-correlation interactions were described by the generalized gradient approximation (GGA) [3] in the form of the Perdew-Burke-Ernzerhof functional (PBE) [4]. A cut-off energy of 400 eV for plain-wave basis sets was adopted and the convergence threshold was 10-5 eV and 5×10-3 eV/Å for energy and force, respectively. The weak interaction was described by DFT+D3 method using empirical correction in Grimme's scheme [5]. The vacuum space was set to be more than 15 Å, which was sufficient to avoid interactions between periodical images.

Quantum chemical studies were performed using DFT implemented in the GAUSSIAN 16 package [6]. Geometry optimization and frequency analysis were performed with the B3LYP hybrid functional [7] at def2svp basis sets. Independent gradient models based on the Hirshfeld partition (IGMH) [8, 9] were performed by Multiwfn 3.8 [10] and VMD v 1.9.3 [11] molecular visualization software. The bonding energies of the IL and VG were calculated as follows: $E_b = E(AB) - E(A) - E(B)$.

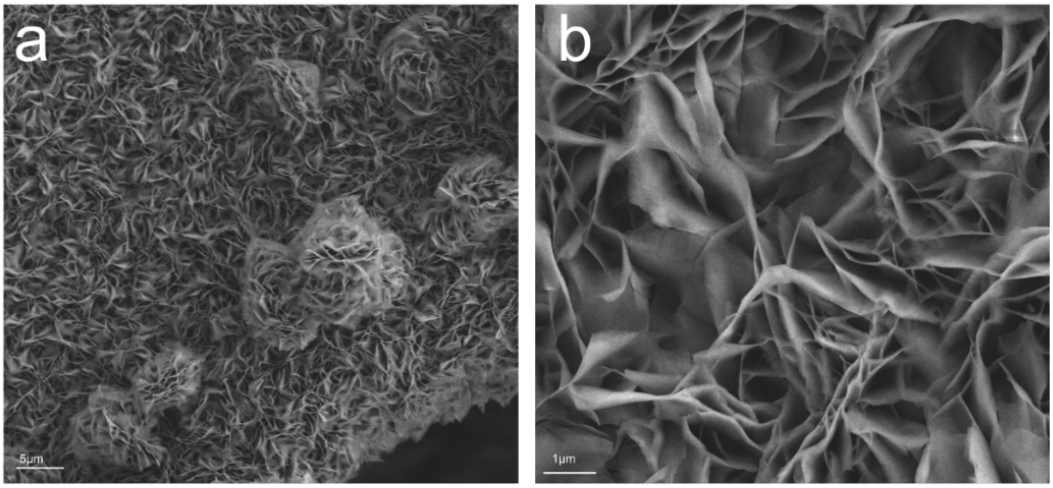

Fig. S1 SEM images of Ni BDC.

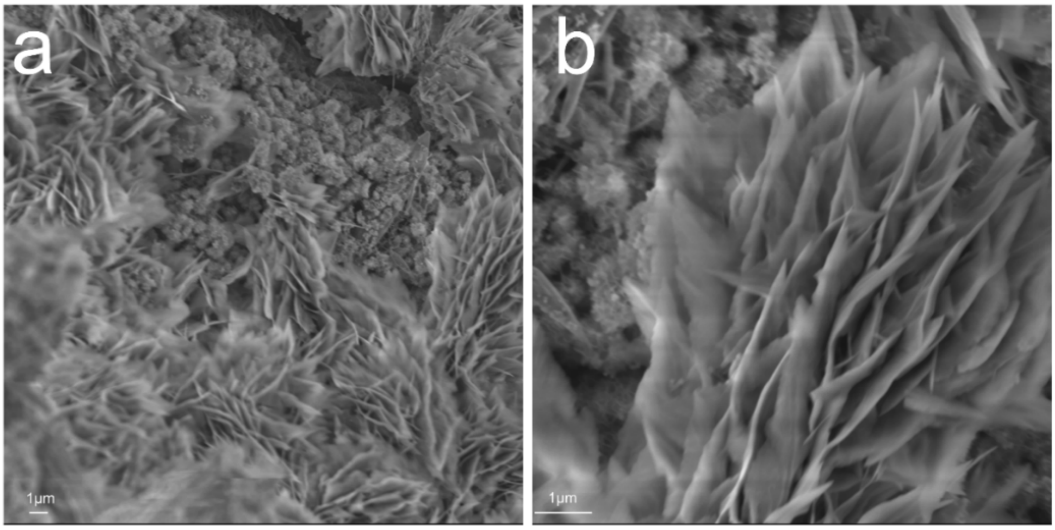

Fig. S2 SEM images of FeNi BDC.

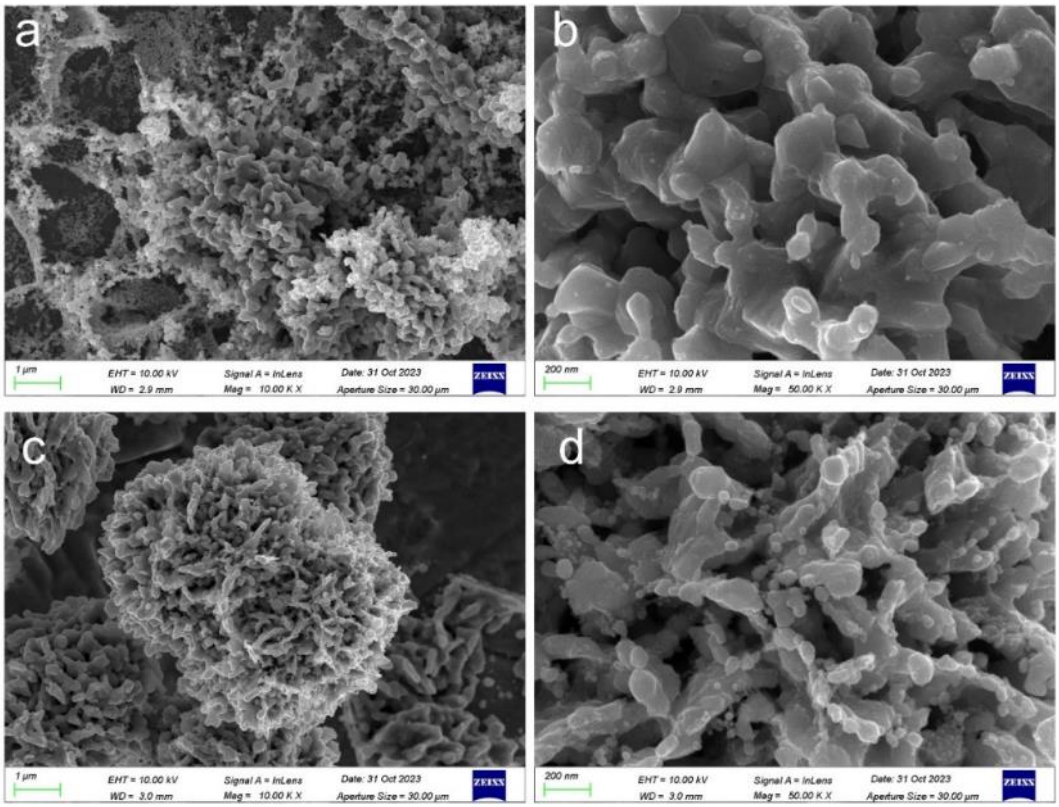

Fig. S3 SEM images of **a** and **b** FeNi@C, **c** and **d** Ni@BDC.

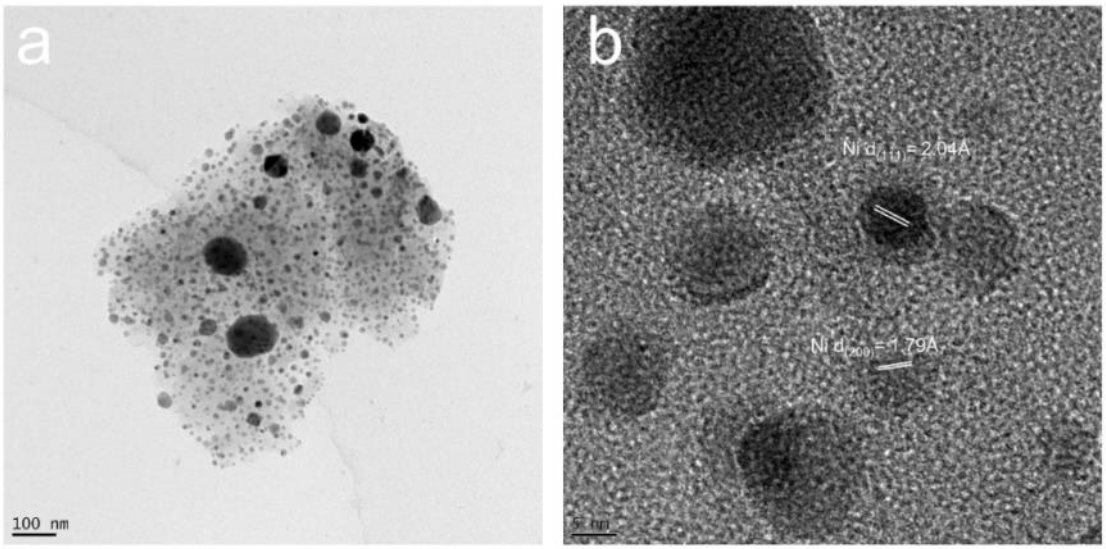

Fig. S4 **a** TEM image of Ni@C. **b** High-resolution TEM image of Ni@C.

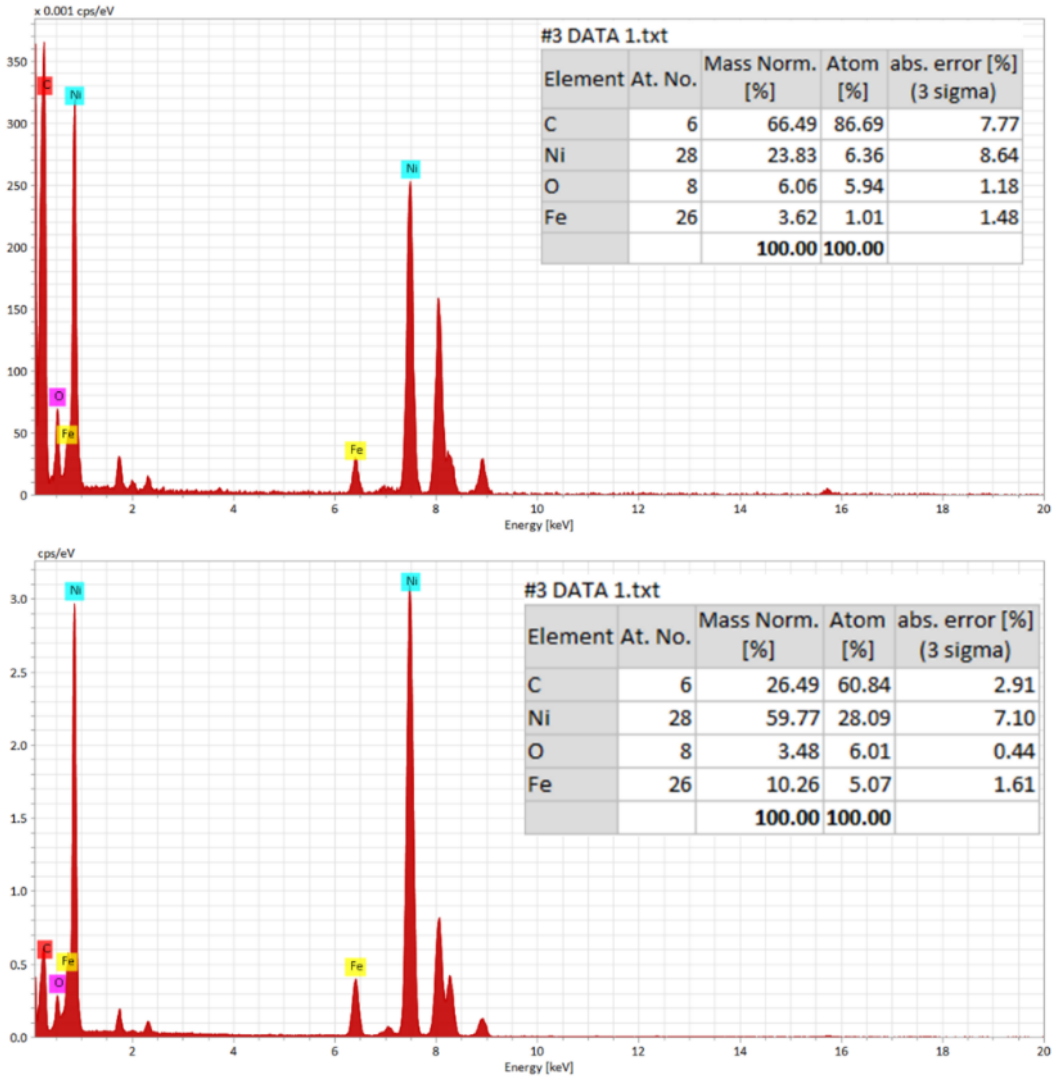

Fig. S5 EDS analysis of different regions on FeNi@C confirms the uniform doping of Fe.

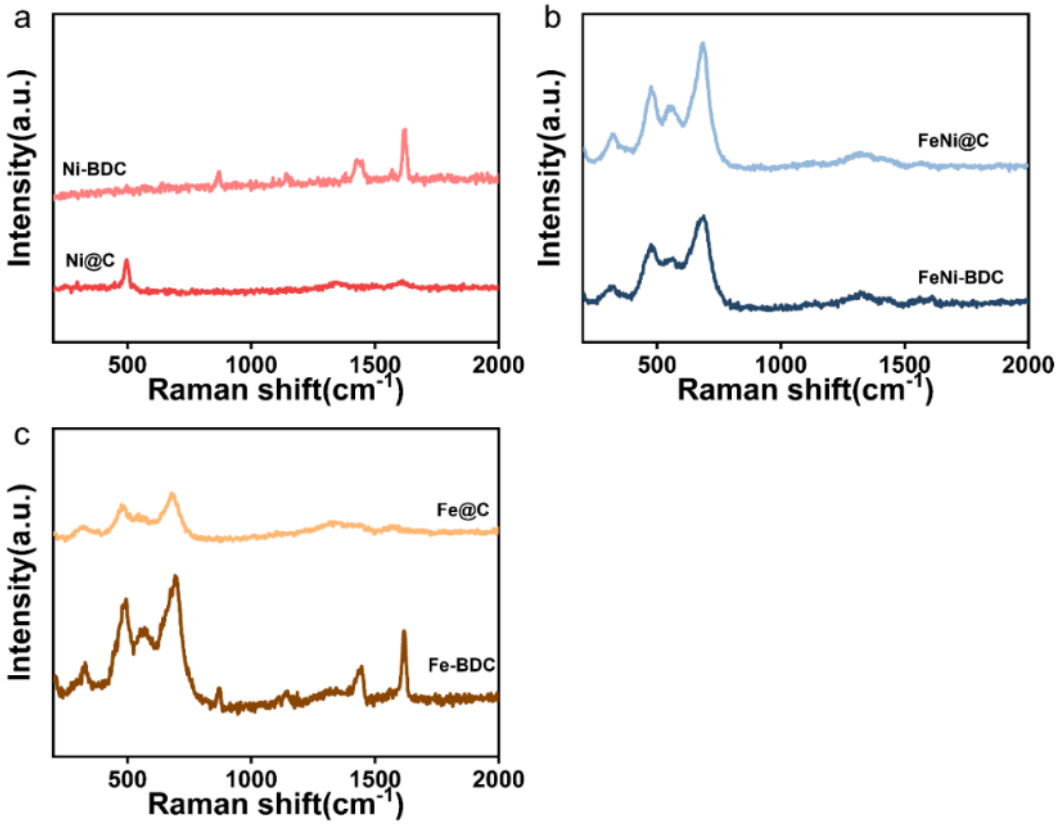

Fig. S6 Comparison of Raman Spectra between Fe_xNi_y-BDC and Fe_xNi_y@C, **a** Ni-BDC and Ni@C, **b** FeNi-BDC and FeNi@C, **c** Fe-BDC and Fe@C.

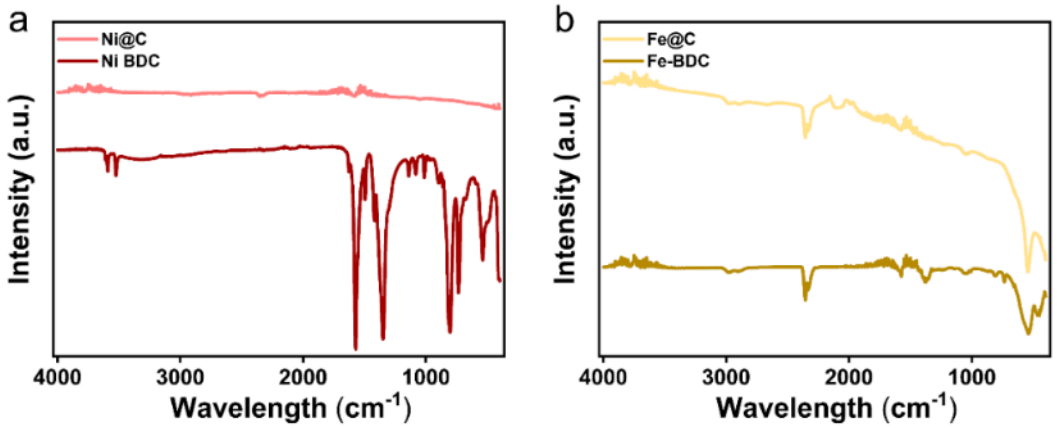

Fig. S7 Overlay of FT-IR spectra of **a** Ni-BDC and Ni@C, **b** Fe-BDC and Fe@C.

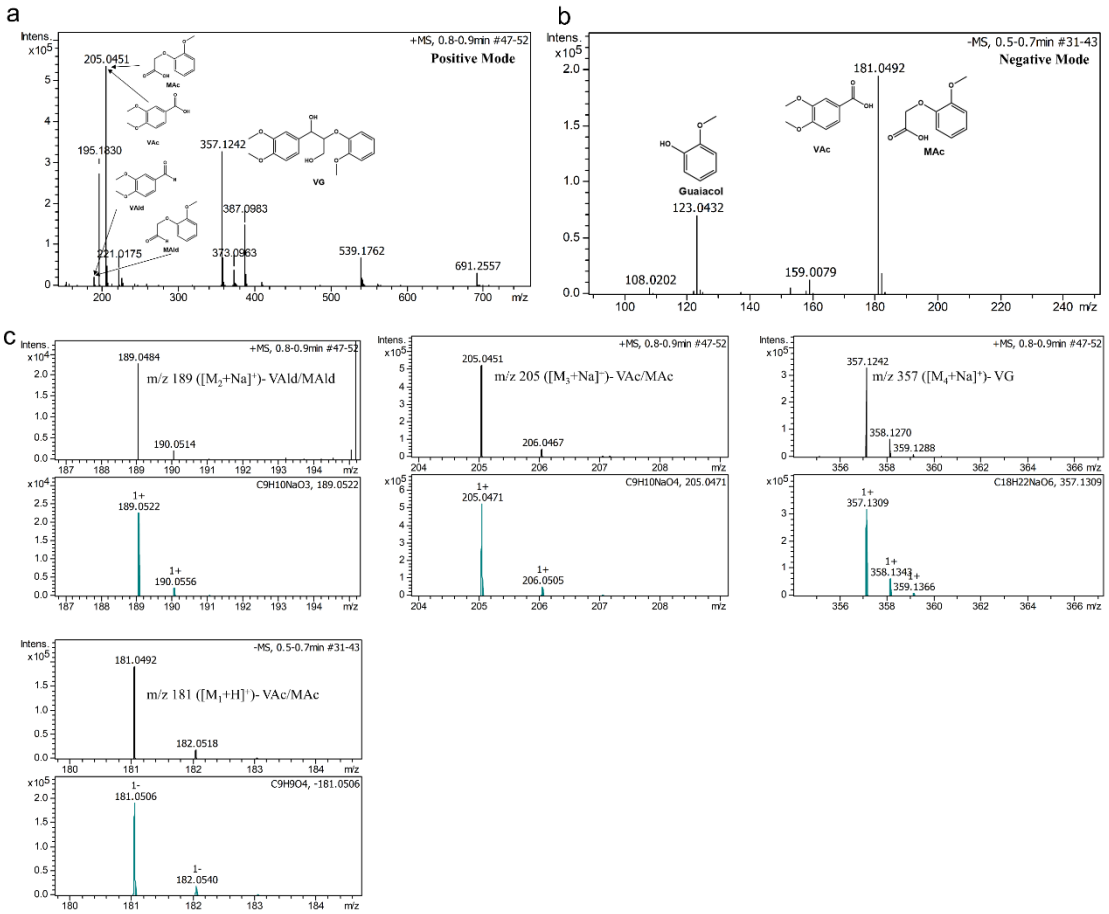

Fig. S8 The LC-MS spectra of the product obtained after electrochemical oxidation of VG, **a** the MS spectrum in negative mode, **b** the MS spectrum in positive mode and **c** the amplified MS spectra obtained in both positive and negative modes.

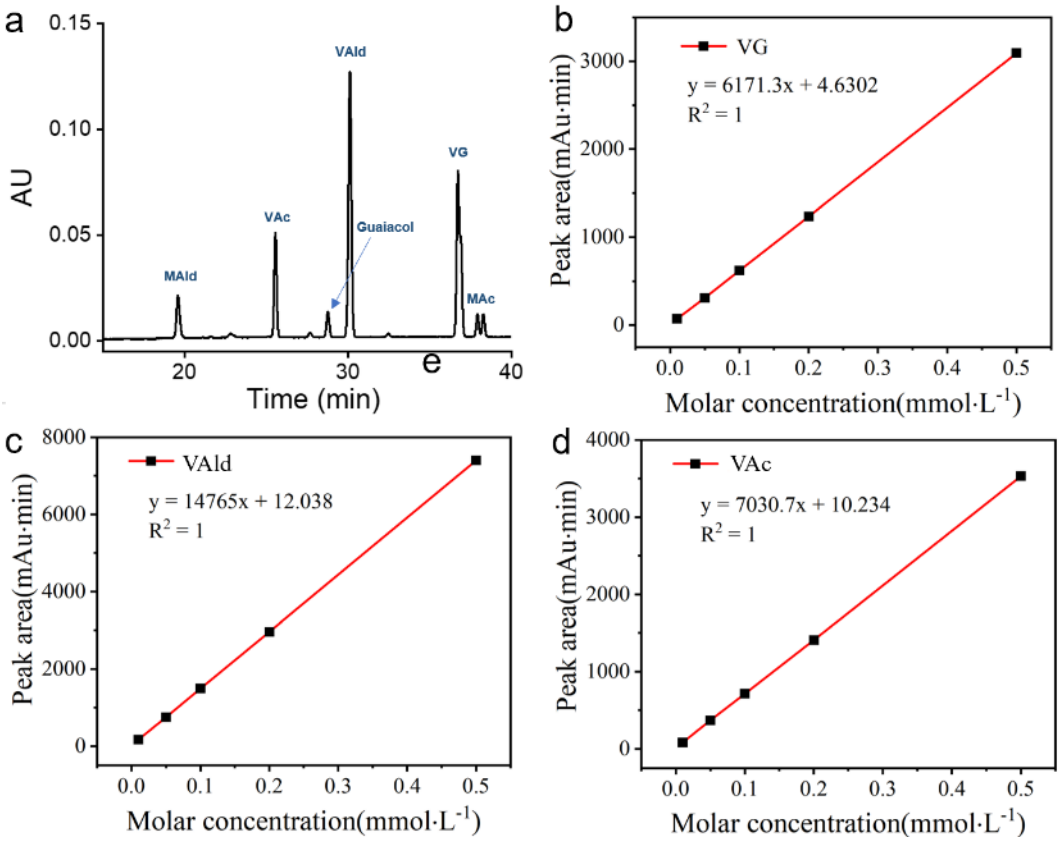

Fig. S9 a The peak signals corresponding to the retention times of reactants and products in HPLC. The standard curves for products and reactants determined by quantitative analysis using HPLC, **b** VG, **c** VAld, **d** VAc.

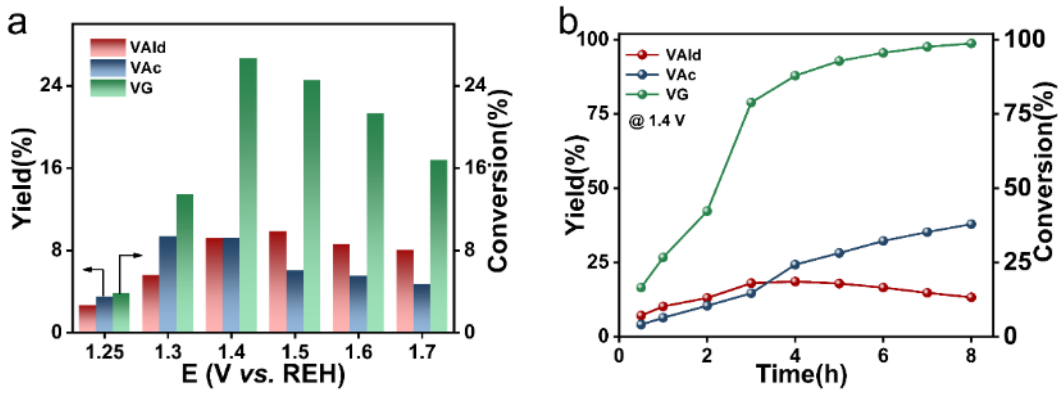

Fig. S10 To determine the optimal reaction conditions, the optimization of both **a** electrolysis voltage and **b** electrolysis time was carried out.

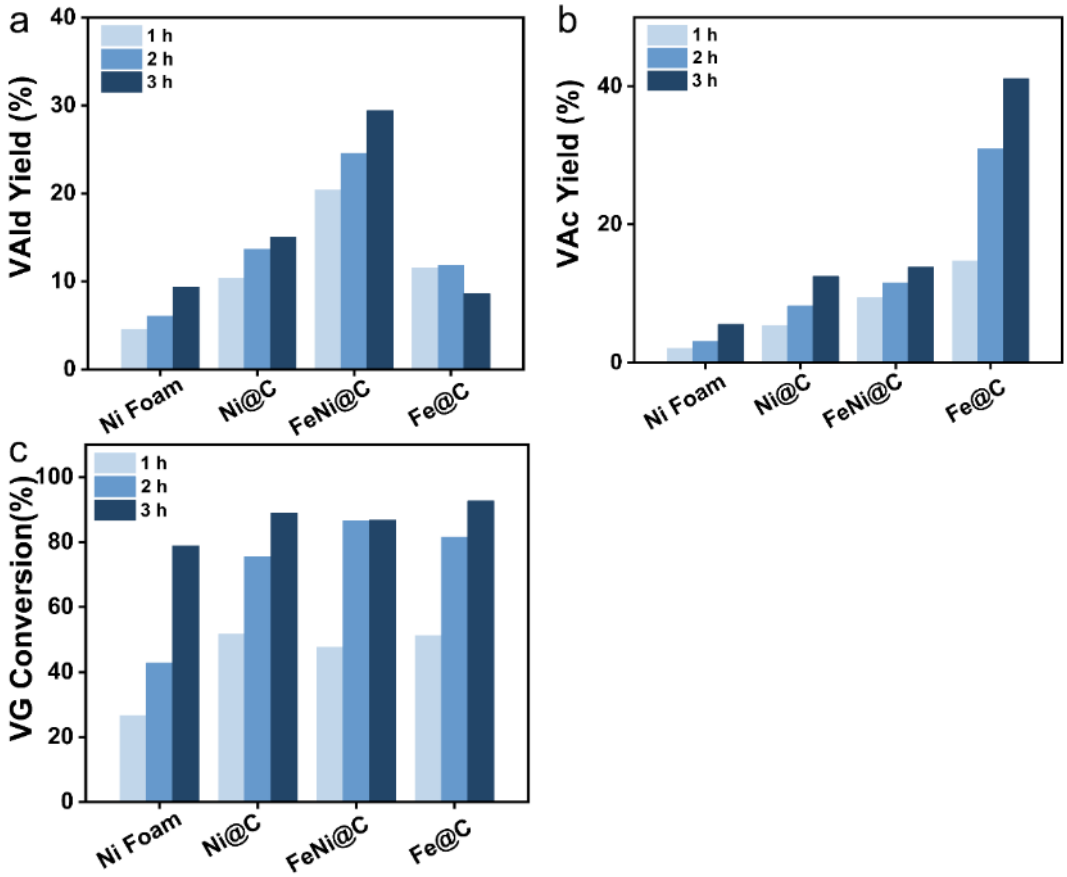

Fig. S11 Quantitative analysis of the temporal variation of reactant and product concentrations under the influence of different electrocatalysts, a VAld, b VAc and VG.

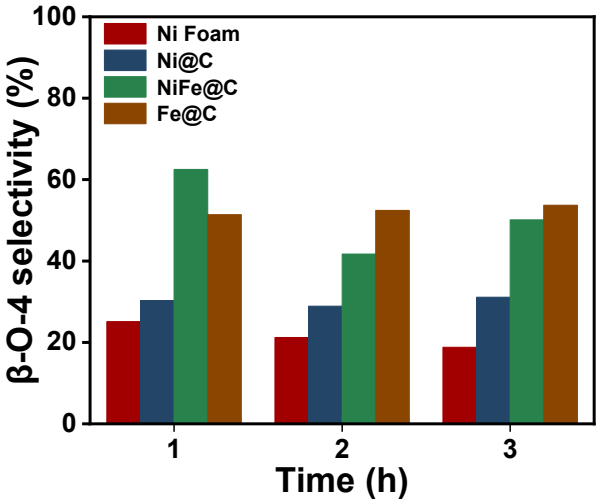

Fig. S12 Selectivity of β-O-4 versus reaction time obtained using chronoamperometry at 1.4V.

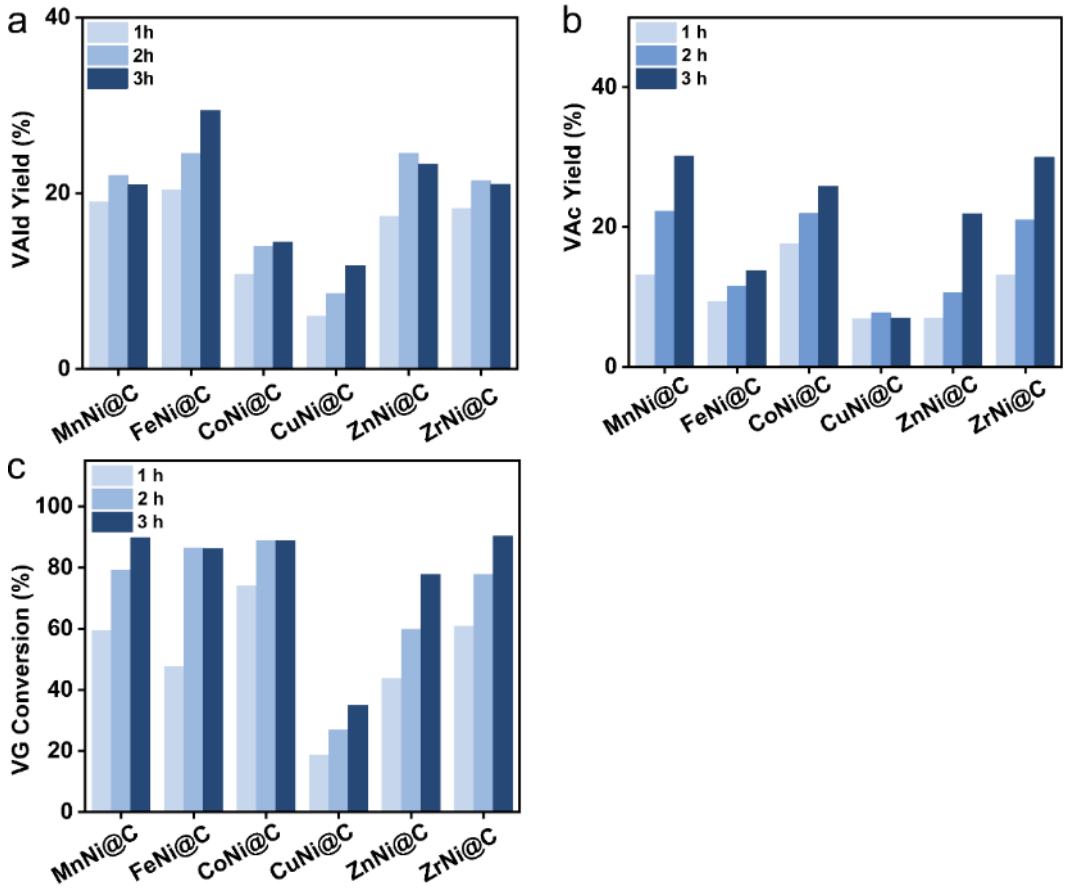

Fig. S13 Quantitative analysis of the temporal variation of reactant and product concentrations under the influence of different Ni-based electrocatalysts, **a** VAld, **b** VAc and **c** VG.

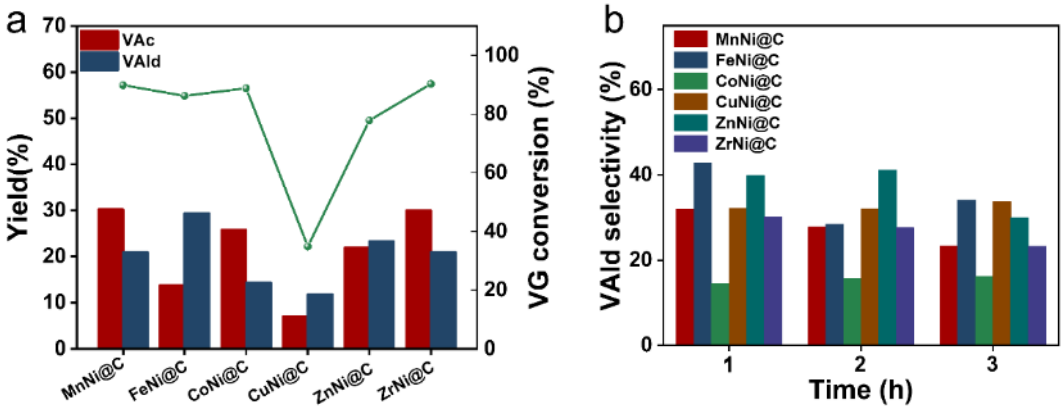

Fig. S14 a Conversions and yield of different Ni- based electrocatalysts determined by HPLC after 3 h of electrolysis at 1.4 V. **b** Selectivity of VAld versus reaction time obtained using chronoamperometry at 1.4 V.

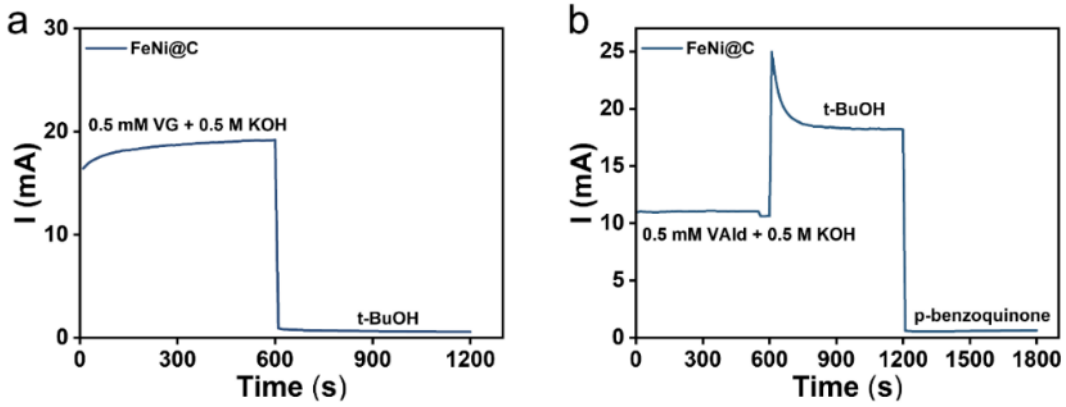

Fig. S15 a Chronoamperometry curve for the oxidation of VG in the presence of tert-butanol. **b** Chronoamperometry curve for the oxidation of VAld with the addition of tert-butanol and p-benzoquinone.

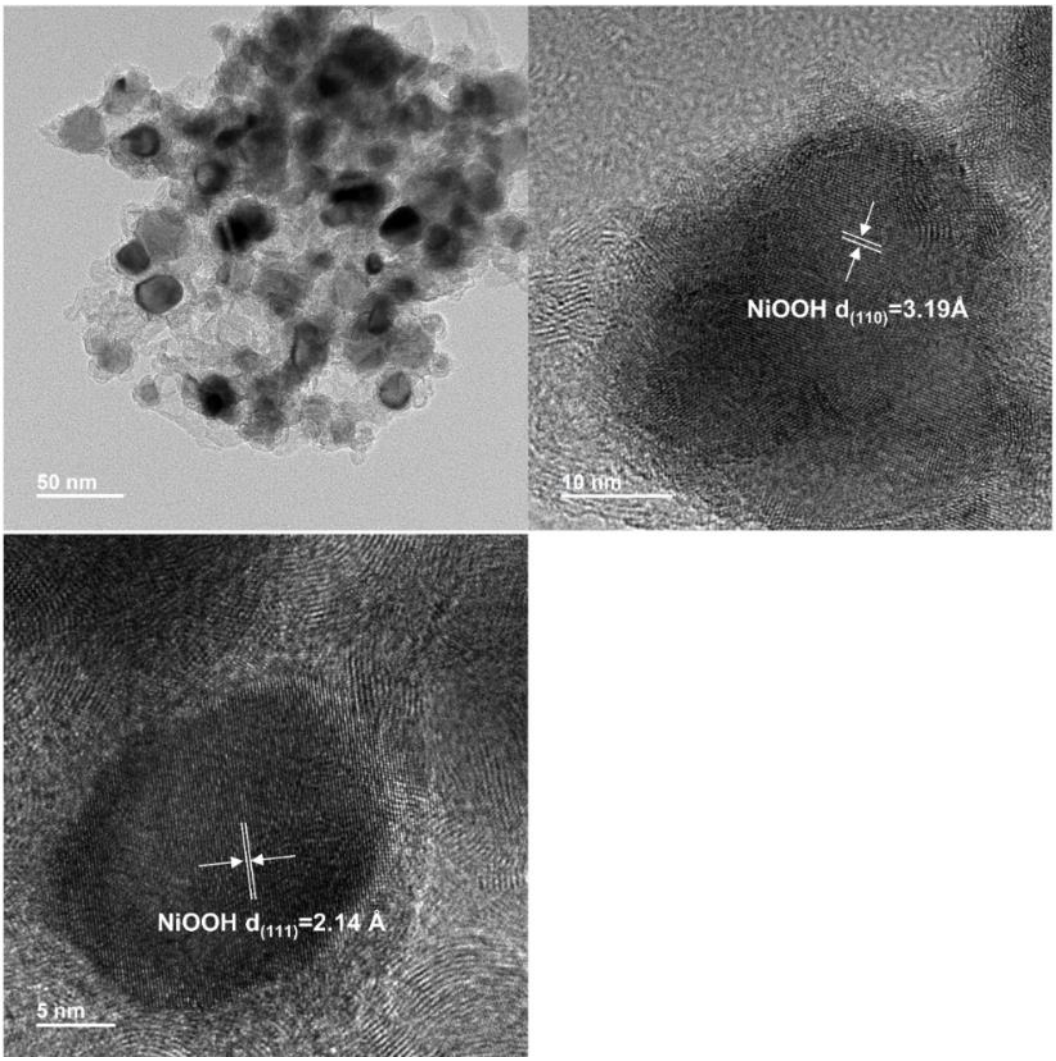

Fig. S16 The TEM image of the reconstructed Ni@C verifies the presence of NiOOH.

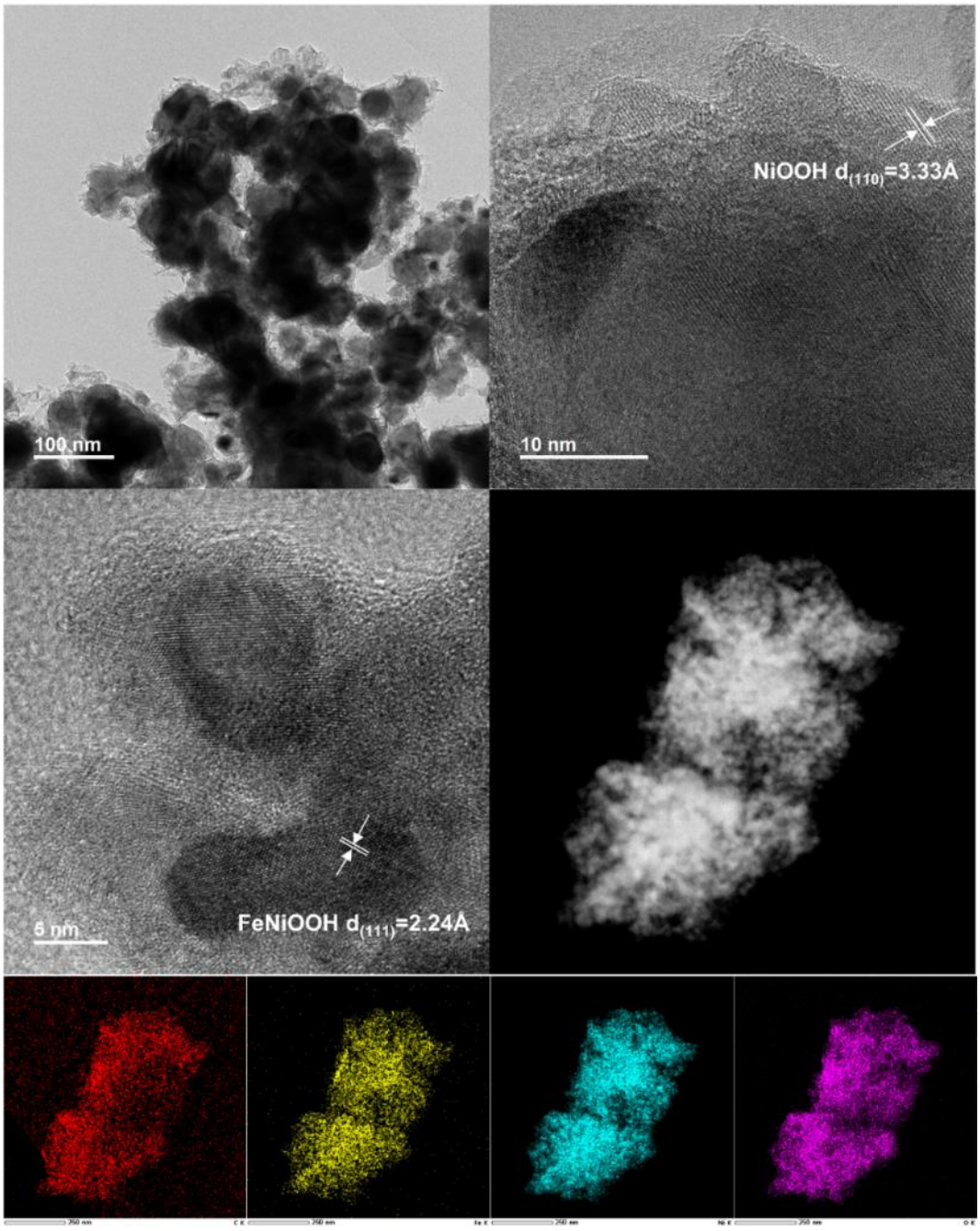

Fig. S17 The TEM image and EDS mapping of the reconstructed FeNi@C verifies the presence of FeNiOOH.

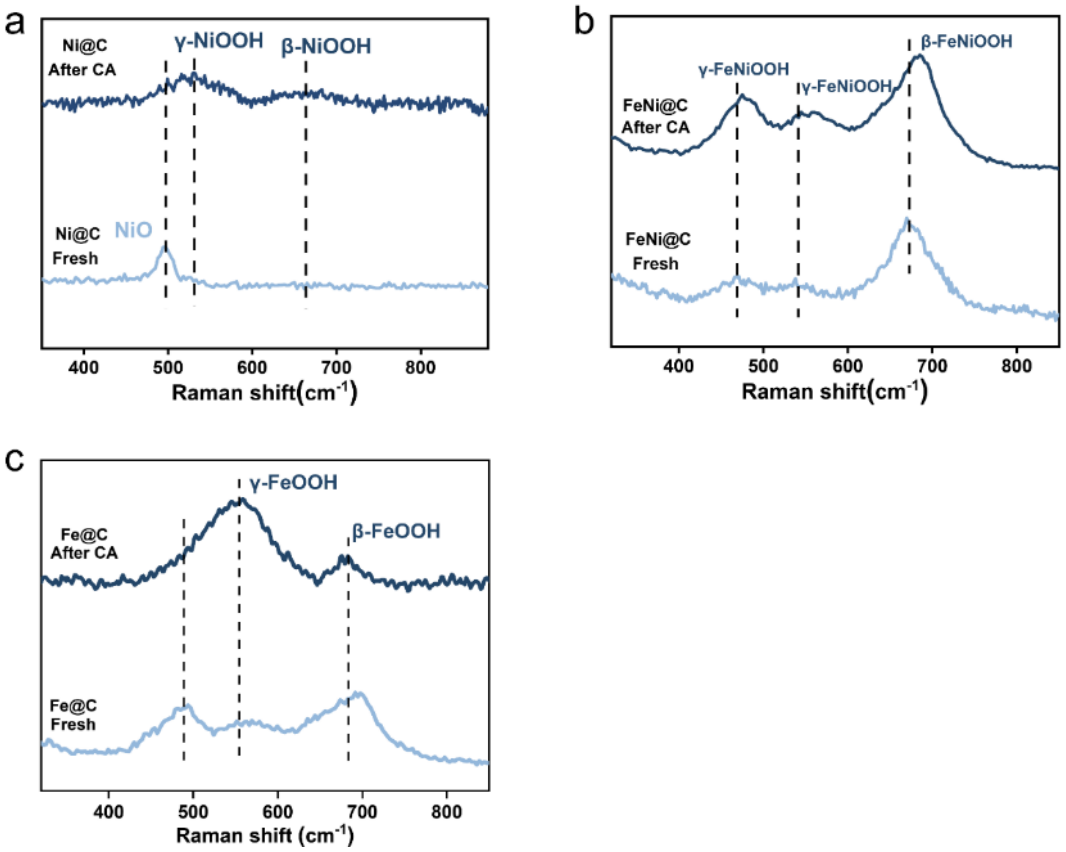

Fig. S18 Raman spectra of FeNi@C and Fe@C before and after 1.4 V electrolysis for 3 h, **a** Ni@C, **b** FeNi@C and **c** Fe@C.

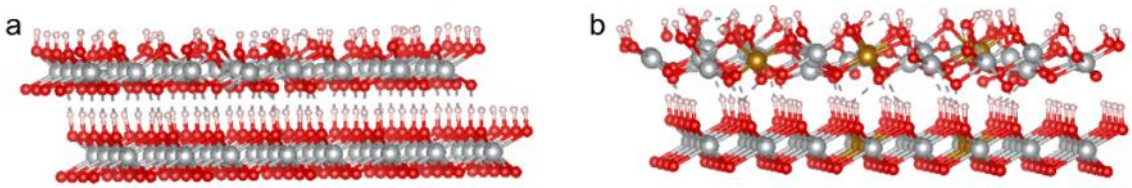

Fig. S19 The atomic structures of the (001) surfaces of **a** Ni@C and **b** FeNi@C are depicted in the figures. In the illustrations, gray, red, pink, and yellow spheres represent Ni, O, H, and Fe atoms, respectively.

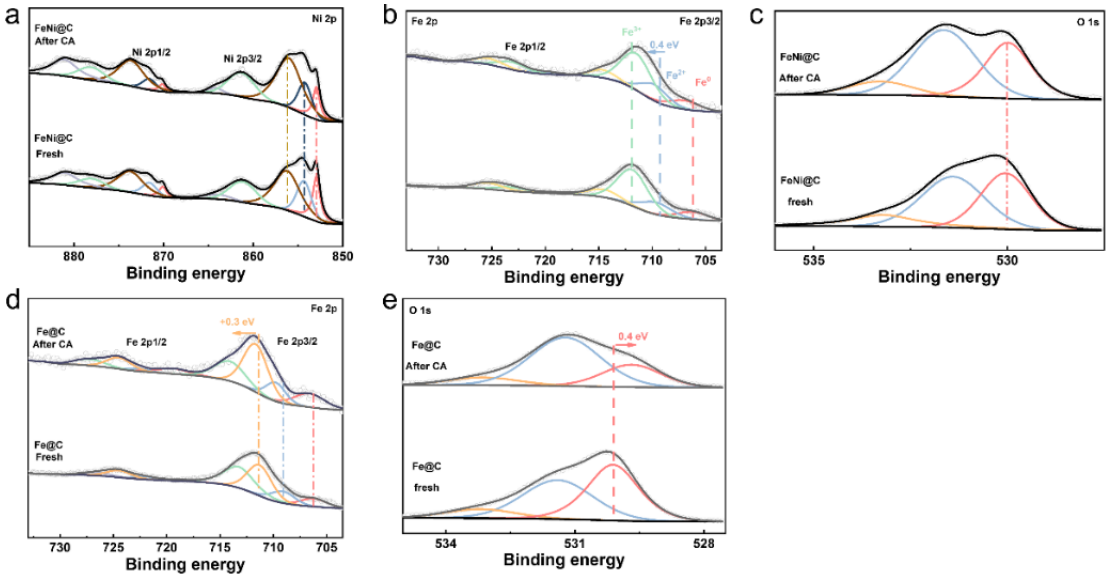

Fig. S20 High-resolution XPS spectra of FeNi@C and Fe@C before and after 1.4 V electrolysis for 3 h, including **a** Ni 2p, **b** Fe 2p, and **c** O 1s for FeNi@C, as well as **d** Fe 2p and **e** O 1s for Fe@C.

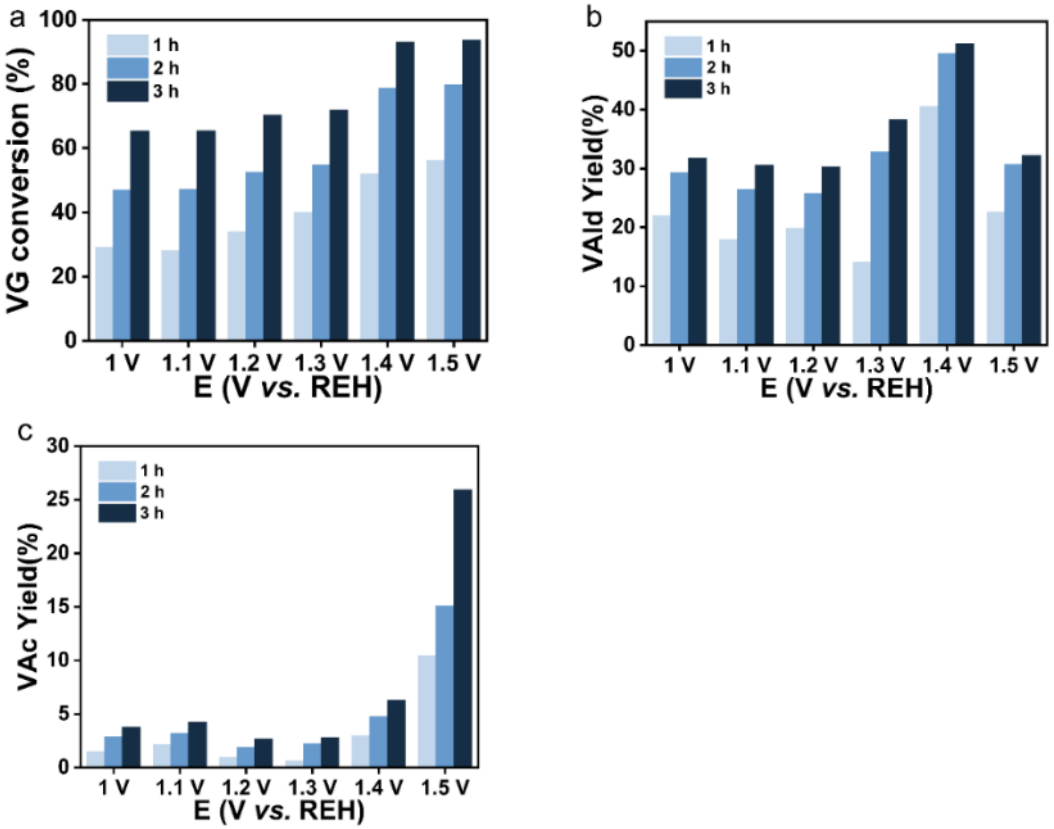

Fig. S21 Optimization of reaction conditions for electrolysis voltage and electrolysis time in AEM electrolysis cells, **a** VG conversion, **b** VAld yield and **c** VAc yield.

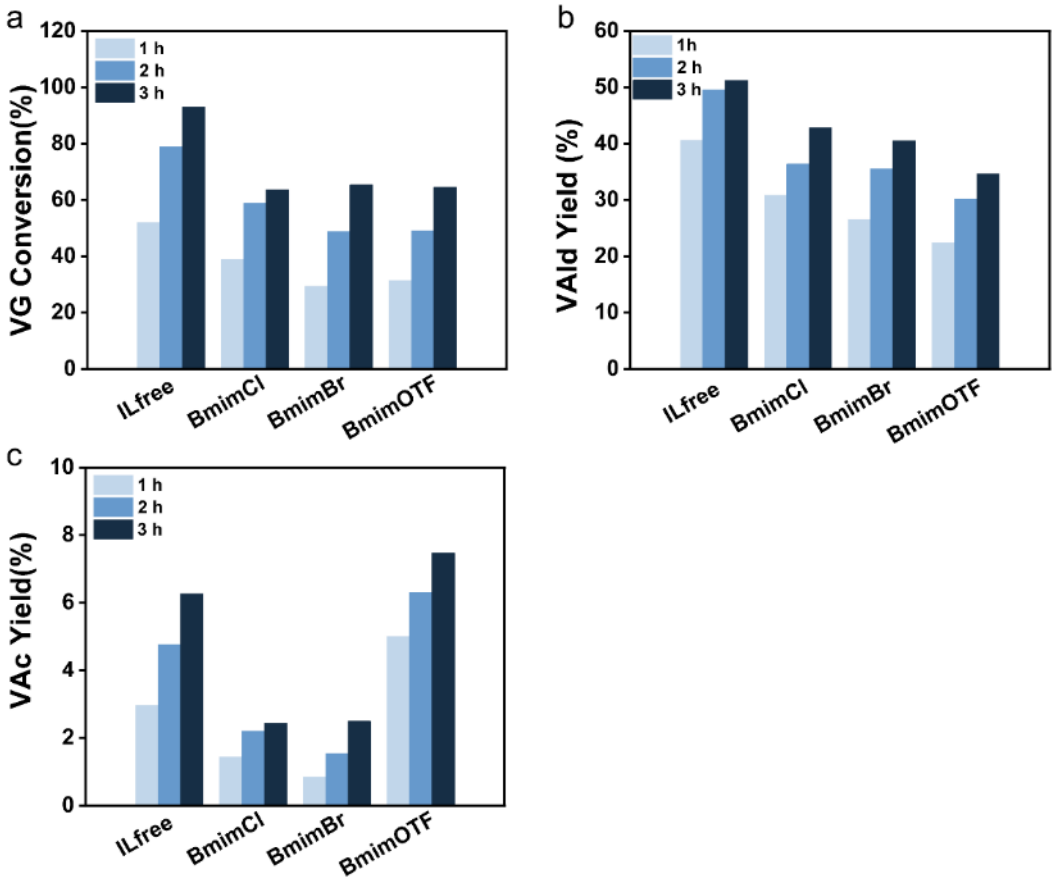

Fig. S22 The impact of the anion of ILs on the reactant conversion and product yield, including **a** VG conversion, **b** VAld yield, and **c** VAc yield.

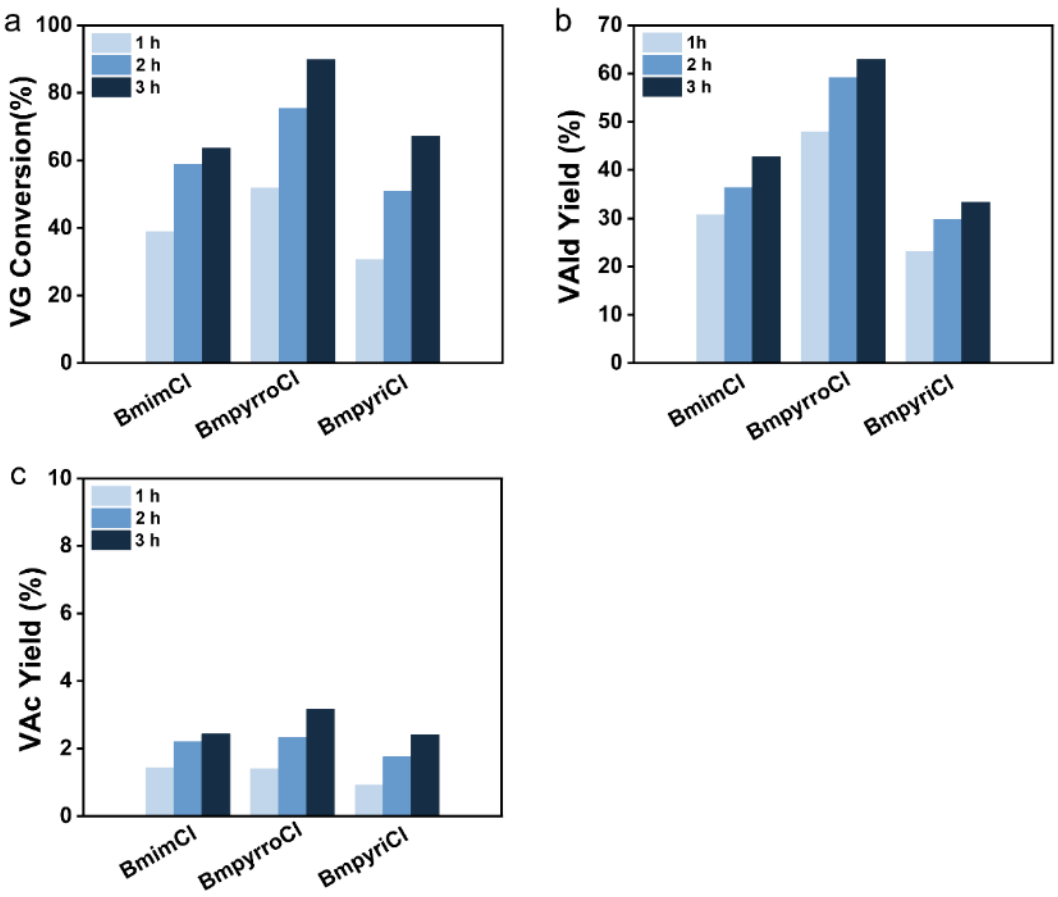

Fig. S23 The impact of the cation of ILs on the reactant conversion and product yield, including **a** VG conversion, **b** VAld yield, and **c** VAc yield.

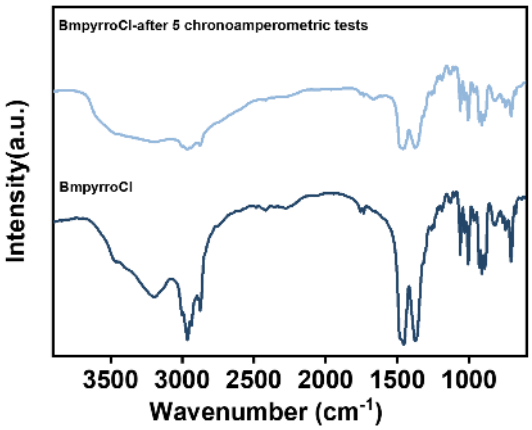

Fig. S24 FT-IR analysis of BmpyrroCl before and after 5 consecutive chronoamperometric tests confirms its stability during a AEM single-cell test**.**

.

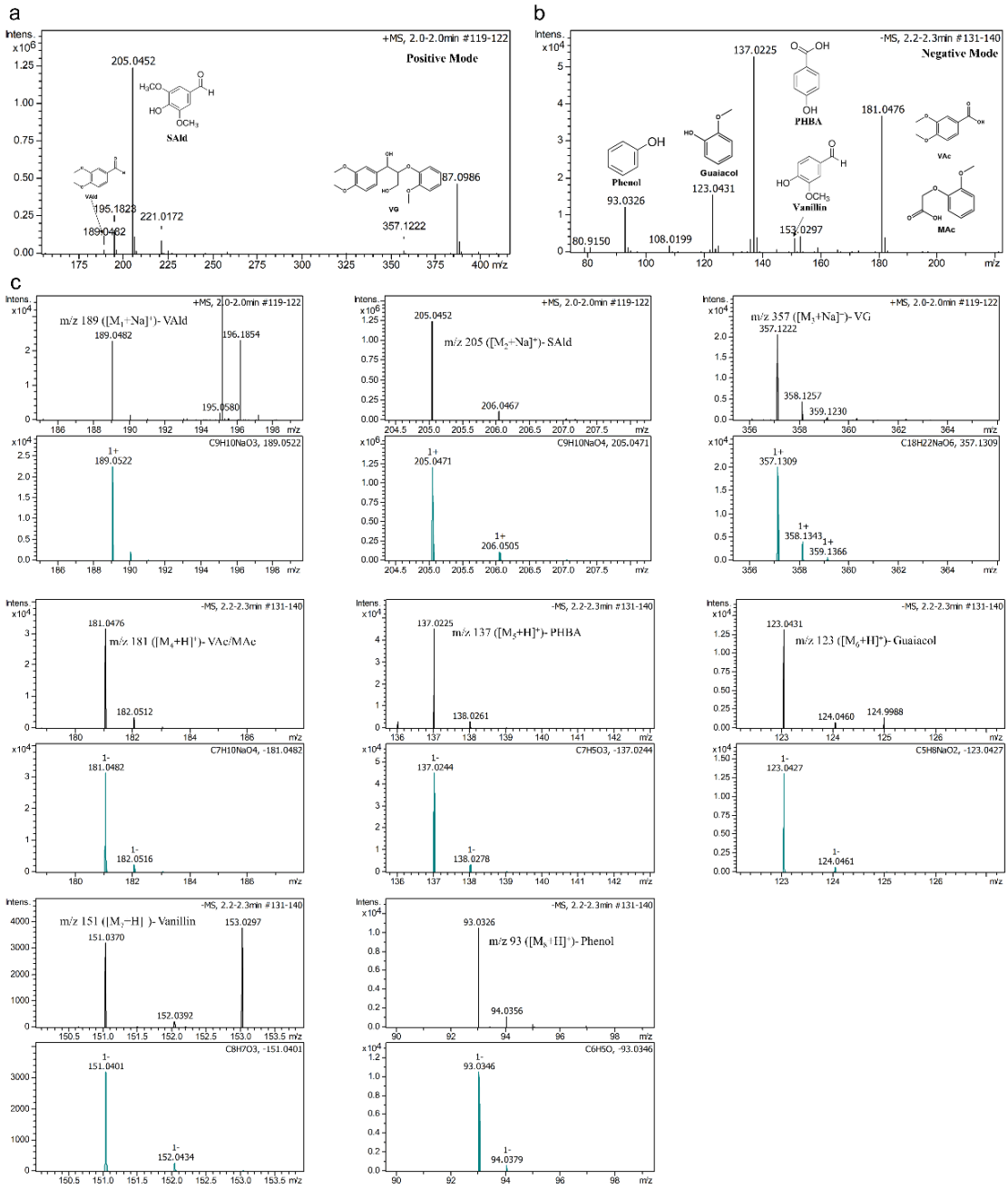

Fig. S25 The LC-MS spectra of the product obtained after electrochemical oxidation of lignin, **a** the MS spectrum in negative mode, **b** the MS spectrum in positive mode and **c** the amplified MS spectra obtained in both positive and negative modes.

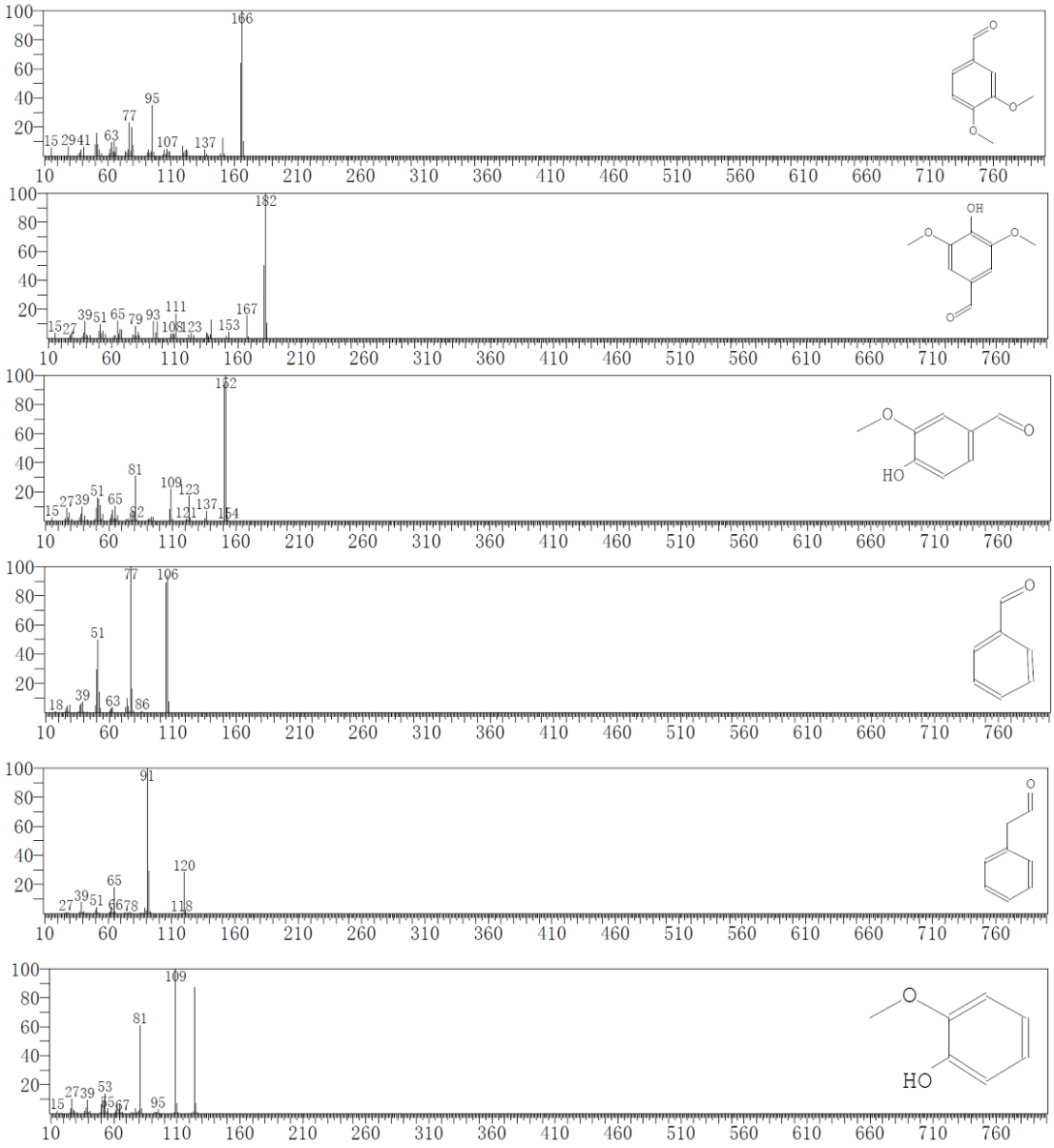

Fig. S26 The GC-MS spectra of the product obtained after electrochemical oxidation of lignin.

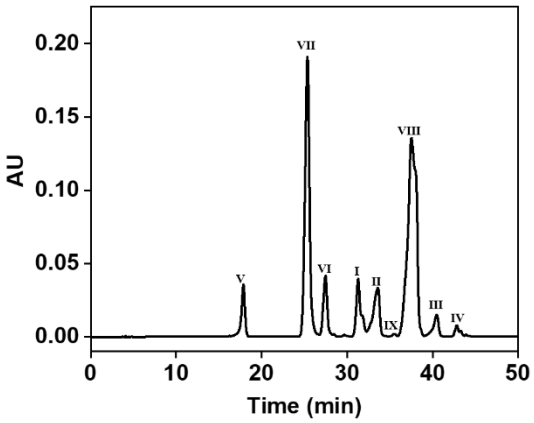

Fig. S27 The peak signals corresponding to the retention times of reactants and products in HPLC.

Table S1 Yield of aromatic compounds from lignin electrolysis.

Depolymerized aromatic compound	Yield (wt.%)
VAld	7.3
Vanillin	5.2
Benzaldehyde	3.2
Phenylacetaldehyde	6
Syringic aldehyde	1.8
Guaiacol	5
VAc	2.2
MAc	2.9
4-hydroxy-benzoicaci	2.4

References

1. G. Kresse and J. Furthmuller, *Comput. Mater. Sci.*, 1996, **6**, 15-50.
2. G. Kresse and J. Furthmuller, *Phys. Rev. B*, 1996, **54**, 11169-11186.
3. J. P. Perdew, K. Burke and M. Ernzerhof, *Phys. Rev. Lett.*, 1996, **77**, 3865-3868.
4. J. P. Perdew, M. Ernzerhof and K. Burke, *J. Chem. Phys.*, 1996, **105**, 9982-9985.
5. S. Grimme, *J. Comput. Chem.*, 2006, **27**, 1787-1799.
6. M. J. Frisch, G. Trucks, H. B. Schlegel, G. E. Scuseria, Robb, J. R. Cheeseman, G. Scalmani, V. Barone, B. Mennucci and G. A. Petersson, 2009.
7. P. J. Stephens, F. J. Devlin, C. F. Chabalowski and M. J. Frisch, *J. Phys. Chem.*, 1994, **98**, 11623-11627.
8. E. R. Johnson, S. Keinan, P. Mori-Sánchez, J. Contreras-García, A. J. Cohen and W. T. Yang, *J. Am. Chem. Soc.*, 2010, **132**, 6498-6506.
9. T. Lu and Q. X. Chen, *J. Comput. Chem.*, 2022, **43**, 539-555.
10. T. Lu and F. W. Chen, *J. Comput. Chem.*, 2012, **33**, 580-592.
11. W. Humphrey, A. Dalke and K. Schulten, *J. Mol. Graph.*, 1996, **14**, 33-38.